Avicenna Journal of Phytomedicine (AJP)

Original article

Synthesis and characterization of Cannabidiol-loaded nanoliposomes and evaluation of their antitumor, antioxidant, and anti-inflammatory effects in a rat model of glioblastoma multiforme

Zahraa Abdulalamir[1,*], Zahra Keshtmand[2]

[1]*Middle Technical University, Al-Mansour Technical Institute, Department of Medical Laboratory Techniques, Baghdad, Iraq*
[2]*Department of Biology, Central Tehran Branch, Islamic Azad University, Tehran, Iran*

Article history:
Received: Feb 25, 2026
Received in revised form: May 25, 2026
Accepted: May 31, 2026
Epub ahead of print

**** Corresponding Author:***
zahraa_abdalmeer6@mtu.edu.iq

Keywords:
Apoptosis
Cannabidiol
Glioblastoma
IL-6
liposomal drug delivery
MDA

Abstract

Objective: Glioblastoma (GBM) remains difficult to treat due to its cellular heterogeneity, diffuse invasion, and the restrictive blood–brain barrier (BBB), all of which limiting drug efficacy. Cannabidiol (CBD), a phytocannabinoid with antitumor, anti-inflammatory, and antioxidant activities, has poor solubility and limited brain penetration. This study aimed to synthesize and characterize cannabidiol-loaded nanoliposomes (CBD-NLs) and evaluate their therapeutic effects in an orthotopic C6 glioma rat model compared with free CBD.

Materials and methods: CBD-NLs were prepared by thin-film hydration and characterized by SEM, TEM, DLS, and FTIR. Adult male Wistar rats (n = 28) were randomized into four groups (n = 7 each): healthy control, glioma model (untreated), free-CBD, and CBD-NL. Endpoints included histopathology (H&E and Cresyl Violet), apoptosis, antioxidant status (Superoxide dismutase (SOD) activity; malondialdehyde (MDA) level, and relative mRNA expression of *TNF-α, IL-6*, *RIPK3*, and *VDAC1* by RT-qPCR (ΔΔCt).

Results: CBD-NLs formed nearly spherical vesicles (~48.6 nm). FTIR confirmed characteristic phospholipid and CBD functional groups, indicating successful non-covalent incorporation of CBD without chemical degradation. Both CBD and CBD-NL improved tumor histology, increased apoptosis, normalized redox status (increased SOD and decreased MDA), and downregulated TNF-α, IL-6, RIPK3, and VDAC1 (vs. glioma model). Notably, CBD-NL consistently outperformed free CBD, achieving greater tumor regression, neuronal preservation, and more pronounced biochemical and transcriptional changes.

Conclusion: Encapsulation of CBD into BBB-permeable liposomes enhanced its antitumor, pro-apoptotic, antioxidant, and anti-inflammatory effects in an orthotopic GBM model. CBD-NL demonstrated superior efficacy over free CBD, highlighting liposomal delivery as a promising strategy to improve molecular-targeted therapies for GBM.

Please cite this paper as:
Abdulalamir Z, Keshtmand Z. Synthesis and characterization of Cannabidiol-loaded nanoliposomes and evaluation of their antitumor, antioxidant, and anti-inflammatory effects in a rat model of glioblastoma multiforme. Avicenna J Phytomed, 2026

Introduction

The World Health Organization Central Nervous System tumour update (WHO CNS5) in 2021 has classed glioblastoma as glioblastoma, Isocitrate Dehydrogenase wild-type (IDH-wildtype), CNS WHO grade 4 (WHO, 2021)This new definition combines microscopic tumor characteristics with molecular markers to provide more accurate diagnosis. Diagnostic features include microvascular proliferation (formation of abnormal new blood vessels), necrosis (areas of dead tumor cells) and genetic changes such as mutation of the Telomerase Reverse Transcriptase (TERT) promoter, amplification of the Epidermal Growth Factor Receptor (EGFR) gene and the chromosomal abnormality of +7/−10 (gain of chromosome 7 and loss of chromosome 10) (Gilard et al. 2021).

This refinement has increased the diagnostic accuracy but also underlines the highly aggressive nature of this tumor and its large biological heterogeneity which are responsible for the clinical challenge in managing glioblastoma (Khalighi et al. 2024; Louis et al. 2021).

Despite the introduction of the Stupp regimen that provides maximal safe surgical resection of the tumor as well as radiotherapy and concomitant and adjuvant temozolomide (TMZ) chemotherapy, the clinical outcomes of glioblastoma have not been satisfactory over the last two decades with incremental therapeutic advances (Weller et al., 2024). Current clinical trials generally report a median overall survival (OS) of approximately 14 to 16 months, with limited survival benefits observed in some subgroups, such as patients with O6-methylguanine-DNA methyltransferase (MGMT) promoter-methylated tumor (Fekete 2024). Survival rates in the real world are usually even lower than in controlled clinical trial populations, because the disease is aggressive and does not respond to available therapies (Price et al. 2024).

The limited and transient therapeutic benefit in glioblastoma is mainly caused by a few biological barriers: the ability of the tumor to widely infiltrate surrounding brain tissue (diffuse invasion), the marked variability between tumor cells (intratumoral heterogeneity), and the fast development of resistance under treatment-related selective pressure (Zaidi et al. 2023). Furthermore, the presence of blood-brain barrier (BBB) greatly limits efficient drug delivery into the central nervous system (CNS), thereby reducing the pharmacologic exposure at the tumor site (Wu et al. 2023).

Therapeutic failure in glioblastoma is a problem on a systems level, not a problem of a single defect. First, poor drug delivery and exposure to the central nervous system are caused by poor penetration and active efflux mechanisms (Angom et al. 2023; Wu et al. 2023). Second, the biology of the tumor is highly resistant, driven by multiple overlapping survival pathways such as the phosphoinositide 3-kinase/protein kinase B/mammalian target of rapamycin (PI3K/AKT/mTOR) pathway and the mitogen-activated protein kinase (MAPK) pathway that maintain growth through compensatory signaling, reducing the efficacy of therapies directed against a single molecular node (Guo et al. 2023). Thirdly, the tumor microenvironment is characterized by low oxygen conditions (hypoxia), dominance of immune-suppressive myeloid cells and an overall downregulation of anti-tumor immunity, all of which creating an environment that is poorly responsive to immune attack (Li et al. 2025; Lin et al. 2024). Finally, glioblastoma is highly resilient as shown by rapid changes in cellular state and phenotype upon cytotoxic treatment allowing constant adaptation and survival (Yabo et al. 2022). Taken together, these barriers imply that advances in delivery modalitiestherapeutics reach and stay in the brain must keep pace with advances in mechanisms of action of the therapies themselves (Wu et al. 2023).

Nanotechnology offers a promising drug-delivery strategy that aligns well with the therapeutic challenges of glioblastoma (Khot et al. 2024). Lipid-based nanocarriers—such as liposomes and nanovesicles—provide several advantages: (a) they can improve the solubility of hydrophobic therapeutic compounds, (b) protect the active molecules from early degradation or metabolism, (c) extend systemic circulation time, (d) allow sustained and controlled drug release, and (e) enhance drug penetration into brain tissue by influencing the BBB and interacting with the tumor microenvironment (Chauhan et al. 2025; Limongi et al. 2021; Rehman et al. 2024). In preclinical neuro-oncology studies, these nanoscale delivery systems have consistently demonstrated improved accumulation of therapeutics within tumors and enhanced treatment efficacy when compared with conventional, non-encapsulated drug formulations (Hersh et al. 2022).

Alongside advancements in drug-delivery systems, cannabidiol (CBD) has progressed from being a simple pharmacological observation to a scientifically justified therapeutic candidate in glioma research (Hasan et al. 2022). CBD is a non-psychoactive cannabinoid but exerts multiple biological actions relevant to tumor control (Bukowska 2024). It regulates cellular oxidative balance (redox homeostasis), suppresses major inflammatory pathways such as Tumor Necrosis Factor-alpha (TNF-α) and Interleukin-6 (IL-6), and disrupts both mitochondrial function and intracellular calcium signaling (Trivedi et al. 2023). These combined effects contribute to promoting programmed cell death (apoptosis) while reducing tumor cell migration and angiogenesis (Gross et al. 2021). Importantly, CBD has also been shown to enhance the sensitivity of glioblastoma cells to temozolomide, the current backbone of alkylating chemotherapy, which reinforces its translational potential in combination treatment strategies (Soroceanu et al. 2022; Yau et al. 2023).

However, the clinical applicability of CBD is limited by its inherently poor pharmaceutical properties. CBD has low aqueous solubility, undergoes extensive first-pass metabolism, and achieves only minimal penetration into the brain, restricting its therapeutic effect (Hossain et al. 2023). Encapsulating CBD within nanoliposomes can directly overcome these challenges (Zapata et al. 2023). Modern liposomal formulations, typically measuring approximately 50–150 nanometers in diameter, enhance its water compatibility, protect the compound from early metabolic degradation, provide more controlled and sustained drug release, and improve delivery across the CNS barriers (Banerjee et al. 2024; Xie et al. 2024). Additionally, recent advancements in nanocarrier platforms—including nanovesicles and nanostructured lipid carriers (NLCs)—have demonstrated improved brain accumulation and excellent biocompatibility (Grifoni et al. 2025). These pharmacokinetic improvements provide exactly the type of delivery enhancement that CBD requires to exert meaningful therapeutic activity within the glioblastoma (GBM) tumor microenvironment (Feng et al. 2024; Rybarczyk et al. 2025).

This study is based on a convergence hypothesis proposing that combining a multifunctional therapeutic compound, CBD, with an intelligent nanoscale delivery system, nanoliposomes, may simultaneously overcome two major therapeutic barriers in GBM: inadequate drug exposure within the CNS and rapid development of treatment resistance. By formulating and characterizing CBD-loaded nanoliposomes, and evaluating their anti-tumor, antioxidant, and anti-inflammatory efficacy *in vivo*, the intention is not only to achieve improved tumor control but also to induce deeper biological modulation—specifically, reducing

necroptotic and inflammatory signaling and restoring redox homeostasis in a tumor known for exploiting these pathways to maintain survival.

Materials and Methods

Animal ethical considerations

All animal procedures complied with international standards for the care and use of laboratory animals (including the EU Directive 2010/63/EU and the AVMA Guidelines for the Euthanasia of Animals, 2020) (Directive 2010), relevant national regulations, and institutional policies. At the end of the experimental period, rats were deeply anesthetized with ketamine (100 mg/kg) and xylazine (10 mg/kg) and humanely euthanized in accordance with AVMA (2020) and EU Annex IV guidelines (Directive 2010).Reporting follows the ARRIVE guidelines; every effort was made to minimize animal suffering and to reduce the number of animals used.

Animals and housing

The study used adult male Wistar rats (220–250 g; n = 28). Animals were acclimatized for one week prior to experimentation and maintained under standard conditions (22 ± 3°C, 12 hr light/12 hr dark, ~70% relative humidity) with *ad libitum* access to standard pelleted chow and water. Routine health checks were performed daily.

Scientific justification

An *in vivo* glioblastoma model is required to study tumor growth within the intact brain microenvironment and to evaluate CNS delivery and efficacy of CBD and CBD-loaded nanoliposomes; these objectives cannot be achieved using non-animal or purely *in vitro* systems.

Anesthesia, surgery, and peri-operative care

Tumor induction was performed by stereotaxic intracranial implantation of C6 glioma cells under general anesthesia with isoflurane. Body temperature was maintained, ophthalmic lubricant was applied, and aseptic technique was used throughout stereotaxy. Post-procedure monitoring included activity, posture, grooming, neurological status, and body weight. Analgesia was provided per veterinary recommendation when indicated, and humane endpoints were predefined (e.g. >20% body-weight loss, severe neurological deficits, and unremitting distress).

After tumor induction and confirmation of glioblastoma development, the animals were randomly assigned to receive one of the designated treatments liposome alone, free CBD, or cannabidiol-loaded nanoliposome (CBD-NL) according to the experimental timeline. All animals were monitored daily for clinical signs, behavioral changes, pain, or distress, and appropriate supportive care (hydration, nutrition, and environmental adjustments) was provided as necessary to maintain welfare throughout the study period.

At the end of the experimental period, rats were deeply anesthetized with ketamine (100 mg/kg) and xylazine (10 mg/kg) and humanely euthanized in accordance with AVMA (2020) and EU Annex IV guidelines (Directive 2010).

Brains were promptly harvested for histopathological and molecular analyses, with transcardial perfusion using saline followed by 10% neutral-buffered formalin performed when needed to ensure optimal tissue preservation. No unexpected deaths occurred during the experiment.

Reduction, refinement, and replacement (3Rs)

Group sizes were determined a priori based on prior variability and expected effect sizes to achieve statistical power while minimizing animal use. Refinements included standardized surgical Standard Operating Procedures (SOPs) peri-operative care, blinded outcome assessment, and use of validated assays to

reduce variability and the need for repeat procedures.

Ethics approval

The experimental protocols were approved by the Animal Care and Use Committee of Islamic Azad University, Central Tehran Branch, Faculty of Basic Sciences (Approval No. 75384/87, Date: 22/3/2021) and all procedures were performed in accordance with the European Directive 2010/63/EU and the AVMA Guidelines for the Euthanasia of Animals (2020).

Induction of glioblastoma

Cell culture

Rat C6 glioma cells (Iran National Cell Bank) were maintained in Dulbecco's Modified Eagle Medium (DMEM) supplemented with 10% newborn calf serum (NCS), 100 U/mL penicillin, and 100 µg/mL streptomycin at 37°C in 95% air/5% CO_2. Cells at ~80–90% confluence were detached with 0.25% trypsin (3 min), washed, centrifuged (1000 rpm, 10 min), and resuspended on ice at 1×10^6 cells/50 µL DMEM (Giakoumettis et al. 2018; Shi et al. 2015).

Stereotaxic implantation

Under isoflurane anesthesia, rats were fixed in a stereotaxic frame. Using a 10-µL Hamilton syringe, 5×10^4 C6 cells in 2.5 µL were injected into the right hemisphere at the following coordinates relative to bregma: AP +1.6 mm, ML −2.0 mm, DV −6.0 mm. The needle was kept in situ for ~2 min to reduce reflux and then slowly withdrawn. Every day the animals were watched. Representative cohorts were sacrificed at predefined endpoints on days 8, 14, 15 and 21 after implantation (Barth and Kaur 2009; Shi et al. 2015).

The post-implantation experimental schedule and histopathological analysis of representative brain sections confirmed the development of glioblastoma. Following stereotaxic implantation of C6 glioma cells, animals were monitored daily for general activity, body weight, grooming behavior, posture, and neurological signs. At the predetermined post-implantation time point, representative animals were sacrificed, and brain tissues were processed for hematoxylin and eosin staining. Successful tumor establishment was verified by the presence of glioma-like histopathological features, including increased cellular density, cellular atypia, tissue disorganization, inflammatory cell infiltration, vacuolization, and degenerative changes in the implanted brain region compared with normal control tissue. After confirmation of tumor establishment, animals were allocated to the treatment groups according to the experimental design (Barth and Kaur 2009; Giakoumettis et al. 2018).

Pre-treatment tumor size was not directly measured by imaging; therefore, treatment initiation was based on the predefined post-implantation timeline and representative histopathological confirmation of tumor establishment.

Preparation and optimization of liposomes (Thin-Film Hydration)

Cannabidiol (CBD) used in this study was obtained as a purified analytical-grade compound from Sigma–Aldrich (Merck KGaA, Germany). The material was not extracted in-house from *Cannabis sativa* L., and therefore no plant collection or herbarium voucher number was applicable. The CBD purity was certified by the manufacturer (≥99%) and used directly for nanoliposome formulation.

The thin-film hydration of nanoliposomes were prepared by. Briefly, phosphatidylcholine (DSPC) and cholesterol were dissolved in chloroform and transferred to a round-bottom flask. The solvent was evaporated on a rotary evaporator under vacuum at 60°C at120 rpm until a uniform thin lipid film was formed. The system was rested under vacuum for ~1 hr to ensure complete solvent removal. The film was then hydrated with 10 mL CBD solution plus 10

mL phosphate-buffered saline (PBS, pH 7.4) and rotated for 1 hr at the same settings to form multilamellar vesicles. Dispersions were transferred to sterile tubes and stored at 4°C prior to size-reduction and assays. Formulations were prepared at varying DSPC:cholesterol ratios (Šturm and Poklar Ulrih 2021).

Particle size by Dynamic Light Scattering (DLS)

Hydrodynamic diameter of CBD-loaded liposomes was measured at 25°C using DLS (Malvern Nano S90, 633 nm). Samples were diluted in filtered PBS to avoid multiple scattering. Each measurement comprised ≥3 runs; size distributions are reported as the intensity-weighted Z-average (nm), as commonly recommended for nanoparticle and liposomal drug-delivery characterization (Danaei et al. 2018; Filippov et al. 2023).

Polydispersity index (PDI)

PDI was computed automatically by the DLS instrument (Malvern) and used as a measure of distribution width (monodispersity).

Electron microscopy Scanning Electron Microscopy (SEM) and Transmission Electron Microscopy (TEM)

Morphology and size were evaluated using SEM (TESCAN) and TEM (Carl Zeiss). For SEM, diluted samples were deposited on conductive stubs, air-dried, and imaged after sputter coating (if required). For TEM, samples were placed on carbon-coated copper grids, allowed to adsorb, wicked, and imaged at calibrated magnifications, as commonly applied for morphological characterization of liposomal and nanoparticle-based drug delivery systems (Filippov et al. 2023; Senjab et al. 2024).

Fourier Transform Infrared (FTIR) spectroscopy

FTIR spectra were recorded on a PerkinElmer instrument over 400–4000 cm^{-1} Attenuated Total Reflectance (ATR) to probe functional groups and drug–lipid interactions. Spectra were acquired for cholesterol, DSPC, blank liposomes, CBD, and CBD-NL, as commonly applied to evaluate functional groups and possible molecular interactions in lipid-based nanocarrier formulations (Oleszko et al. 2015; Xie et al. 2024).

Experimental groups

Rats (n = 28) were randomized into four groups (n = 7 each):

- Healthy control: no induction, no treatment.
- Glioma model: intracranial C6 implantation only.
- GBM + CBD: glioma model + CBD (1 µL) oral gavage for 30 days.

GBM + CBD-NL: glioma model + CBD-NL (1 µL) oral gavage for 30 days.

Tissue sampling

The rats were deeply anaesthetized with ketamine-xylazine and killed after 30 days of treatment according to the approved protocol. Brains were removed and processed for histology.

Brain histology (Tissue processing)

Fixation and processing

Within 24 hr after the final treatment, animals were anesthetized, and brain tissues were excised, rinsed with saline, weighed, and fixed in 10% neutral-buffered formalin for 24–72 hr. Fixed tissues were processed through standard histological procedures, including dehydration in graded ethanol, clearing with xylene, paraffin infiltration and embedding, sectioning at 5 µm, deparaffinization, and rehydration. Routine hematoxylin and eosin (H&E) and Cresyl Violet (Nissl) staining were then performed according to established laboratory protocols (Fischer et al. 2008; Hammond 2023).

Histological quantification of viable and apoptotic cells

Viable and apoptotic cells were evaluated microscopically in stained brain sections. Viable cells were identified in Cresyl Violet-stained sections based on preserved cellular morphology, intact nuclei, and clear Nissl staining. Apoptotic cells were identified morphologically in H&E-stained sections according to characteristic features, including cell shrinkage, nuclear condensation/pyknosis, cytoplasmic shrinkage, and apoptotic body formation. Cell counts are expressed as percentages relative to the total number of counted cells in the examined microscopic fields, as previously described (Elmore 2007; Doonan and Cotter 2008).

Antioxidant assays

Brain tissue samples were homogenized in cold phosphate-buffered saline and centrifuged to obtain the supernatant for biochemical analysis. The levels of malondialdehyde (MDA), superoxide dismutase (SOD) activity, and total antioxidant capacity (TAC) were measured using commercial assay kits obtained from Padgene Teb, Zellbio GmbH brand, according to the manufacturer's instructions. MDA was determined as an index of lipid peroxidation based on the formation of a colored complex and expressed as kit-recommended units. SOD activity was assessed according to the inhibition of superoxide radical–dependent reactions and expressed as enzyme activity units. TAC was measured based on the total reducing/antioxidant capacity of the sample. Absorbance was read using an autoanalyzer or spectrophotometric plate reader at the wavelengths recommended by the kit protocol. Results were normalized to tissue protein concentration where applicable and reported according to the manufacturer's instructions.

Inflammatory markers and gene-expression analysis

The relative mRNA expression levels of *RIPK3*, *TNF-α*, *IL-6*, and *VDAC1* were quantified in brain tissue using SYBR Green-based real-time PCR. Total RNA was extracted under RNase-free conditions using RNX-Plus reagent, and RNA purity and concentration were assessed spectrophotometrically. cDNA was synthesized using the RevertAid First Strand cDNA Synthesis Kit according to the manufacturer's instructions. PCR reactions were performed in duplicate using gene-specific primers as shown in Table 1, SYBR Green master mix, normalized cDNA template, and nuclease-free water. Melt-curve analysis was used to confirm amplification specificity. Relative gene expression was normalized to GAPDH and calculated using the $2^{-}\Delta\Delta Ct$ method, with the control group used as the calibrator (Livak and Schmittgen 2001)

Table 1. Primer sequences used for RT-qPCR analysis in the present study

Gene	Primer	Sequence 5′→3′	Reference
GAPDH	Forward	AGGTCGGTGTGAACGGATTTG	Designed in this study
	Reverse	TGTAGACCATGTAGTTGAGGTCA	
IL-6	Forward	TCTGCTCTGGTCTTCTGGAGT	Designed in this study
	Reverse	GAGAGCATTGGAAGTTGGGGT	
TNF-α	Forward	ATCCGAGATGTGGAACTGGC	Designed in this study
	Reverse	TTTGCTACGACGTGGGCTAC	
RIPK3	Forward	CTAGCTCCCGATGTCTTCTGT	Designed in this study
	Reverse	TTCACCATAGCCTTCACCTCC	
VDAC1	Forward	CGCCTAACACCGGGAAAAAAA	Designed in this study
	Reverse	CAAAGTTGCTCTGGGTCACTC	

Statistical analysis

Statistical analyses were conducted in SPSS v22 and GraphPad Prism. Data are expressed as mean ± SD (or SEM where specified). Before group comparisons, data distribution was assessed for normality and variance homogeneity was evaluated. Since the analyzed variables showed an approximately normal distribution with acceptable homogeneity of variance, parametric analysis was performed. One-way ANOVA was used to compare groups, followed by Tukey's HSD *post-hoc* test for multiple comparisons. A value of $p<0.05$ was considered statistically significant. For qPCR, group differences were based on the ΔΔCt framework (2^{-}ΔΔCt). All qPCR reactions were performed in duplicate; cDNA concentrations were normalized prior to amplification.

Results

Results of the synthesis and identification of CBD-NL Morphological Assessment by SEM and TEM

Morphology and particle size were evaluated using SEM and TEM. Representative micrographs are provided in Figure 1 (a and b). The images show CBD-NL appearing as aggregated, spherical vesicles with a characteristic particle size in the ~50 nm range under the imaging conditions applied.

Dynamic light scattering (DLS) was used to reliably quantify the submicron particle-size distribution of the lipid nanocarriers. The DLS trace for the CBD-NL dispersion in Figure 1 (c) shows a characteristic hydrodynamic diameter of approximately 48.6 nm, indicating nanoscale vesicles appropriate for brain-delivery applications under the conditions tested.

FTIR spectroscopy (assignment of diagnostic bands)

The FTIR graphs obtained for cholesterol, DSPC, liposome, CBD, and the CBD-NL are presented in Figure 2.

The peaks corresponding to bending and deformation of CH_2 bonds appear in the 1389–1036 cm^{-1} region, and the peaks corresponding to aromatic ring C–C stretching appear at 1517 cm^{-1}—all of which are related to cholesterol. Peaks corresponding to the P–O bond are observed in the 722–826 cm^{-1} region, while bands corresponding to P=O stretching appear at 1243 cm^{-1}, and C–N bonds appear in the 1000–1350 cm^{-1} region; these peaks indicate DSPC interactions.

The spectrum of the liposome shows the main characteristic bands, especially those arising from symmetric and antisymmetric P=O stretching vibrations at 1045 and 1214 cm^{-1}. CH_2 bending appears around 1749 cm^{-1}, carbonyl C=O stretching at 1749 cm^{-1}, and O–H stretching and bending at 3478 and 1645 cm^{-1}, respectively.

CBD interactions were also identified through the presence of peaks at 2400–3400, 1643, 1062, 756, and 849 cm^{-1}, corresponding respectively to the carboxylic acid group, R–CO–NH_2 bond, R–O–R bond, C–Cl bond, and out-of-plane aromatic bending. The presence of carboxylic acid functional groups near 2410 cm^{-1} and C–Cl near 748 cm^{-1} attributable to CBD within the liposome structure can be considered confirmation of the successful loading of the drug into the liposome.

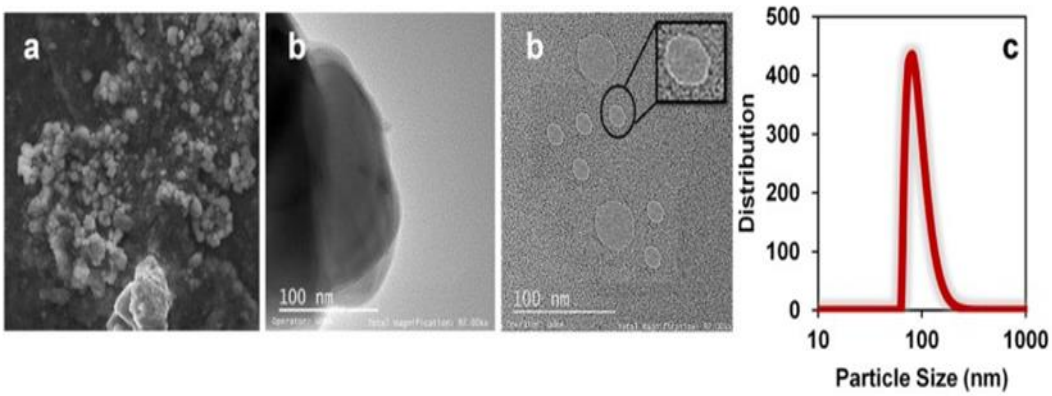

Figure 1. (a) SEM micrograph of cannabidiol-loaded nanoliposomes; (b) TEM micrograph of cannabidiol-loaded nanoliposomes; (c) DLS size-distribution profile of the cannabidiol-loaded liposome dispersion. Measurements were performed in triplicate.

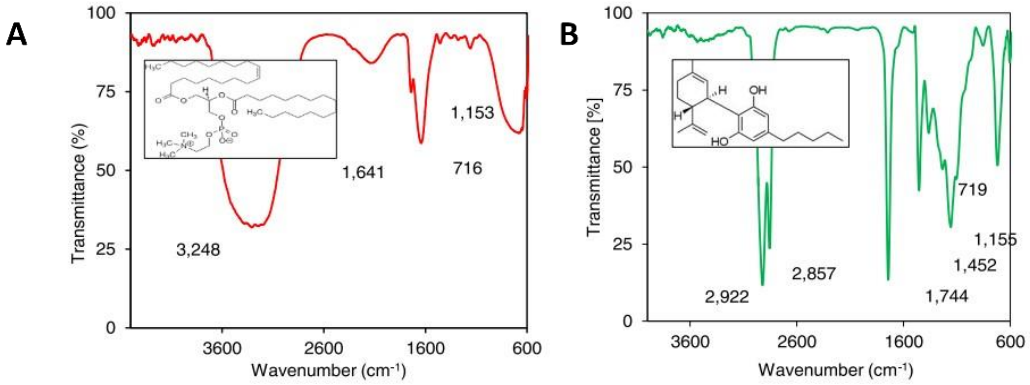

Figure 2 .FTIR spectra of the formulation components. A: phospholipid/cholesterol reference (blank liposome) showing ν(C–H) at ~2922/2857 cm^{-1}, ν(C=O) at ~1744 cm^{-1}, δ(CH_2) at ~1452 cm^{-1}, ν(P=O) around ~1240–1214 cm^{-1}, ν(P–O–C) ~1155–1060 cm^{-1}, and (CH_2) rocking near ~719 cm^{-1}. B: cannabidiol (CBD) with a broad O–H stretch (~3248–3478 cm^{-1}), aromatic C=C (~1641–1600 cm^{-1}), and C–O/ring modes ~1150–1050 cm^{-1}. In the CBD-loaded liposome, these bands are retained with minor shifts, consistent with drug–lipid interactions and encapsulation. Measurements were performed in triplicate.

Histopathological results of brain tissue

Figure 3 presents transverse sections of rat brain tissue from the glioblastoma model (induced with C6 glioma cells) treated with liposome, with CBD, and with CBD-NL, stained with H&E.

In line with Figure 3, the cancer (glioma) group shows increased cellular irregularity, tissue degeneration, higher density of inflammatory cells, and vacuolization relative to the other groups, whereas the CBD-NL, group exhibits improvement in these histopathological features.

In Figure 4, the percentage of apoptotic cells in rat brain tissue from the glioblastoma model (induced with C6 glioma cells) treated with liposome, CBD, and CBD-NL, is shown. The proportion of apoptotic cells increased significantly in all three treatment groups. Notably, the CBD-NL, group showed a significantly higher apoptotic fraction compared with nanocarrier alone and drug alone (approximately ~4-fold and ~2-fold, respectively), and the drug-alone group exceeded the nanocarrier-alone group by roughly ~2-fold ($p<0.001$).

As showed in Figure 5 the Cresyl Violet (CV) staining of rat brain tissue from the

glioblastoma model (induced with C6 glioma cells) treated with liposome, CBD, and CBD-NL. Based on this Figure, neuronal density shows a relative increase in the treated groups compared with the diseased (glioma) group.

In CV staining, the percentage of viable cells in brain tissue of glioblastoma-bearing rats treated with the CBD-NL was reduced compared with rats treated with blank nanoliposome and with CBD alone ($p<0.001$) as shown in Figure 6.

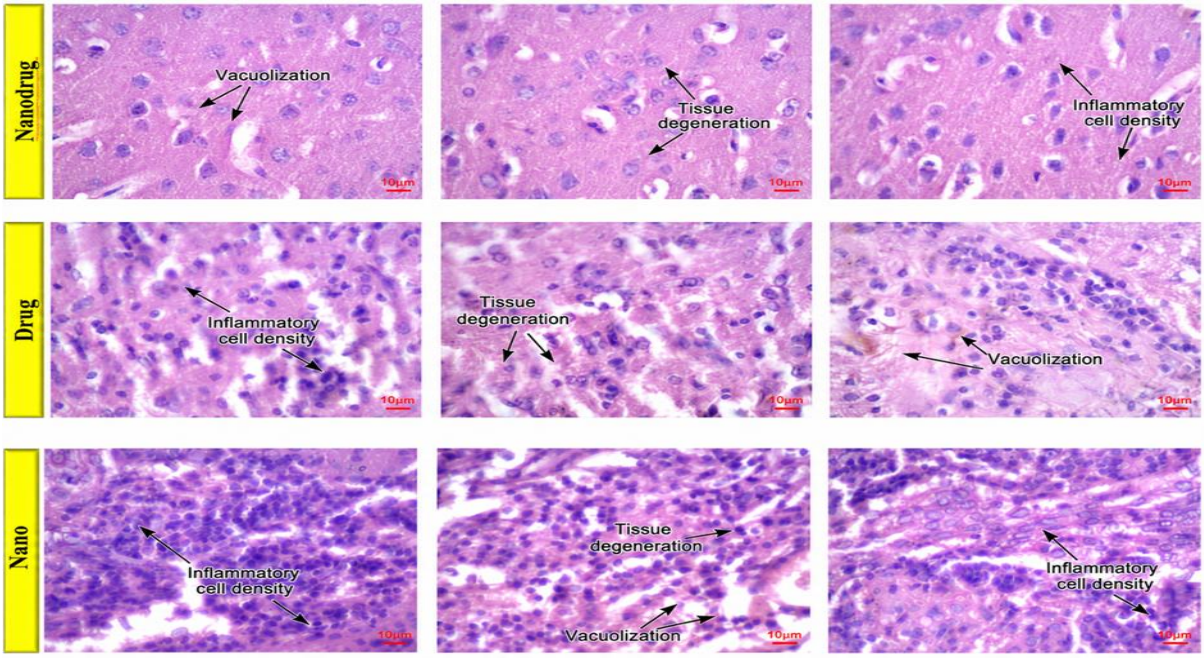

Figure 3. H&E-stained transverse sections of rat brain tissue from glioblastoma-bearing rats treated with blank nanoliposome (Blank-NL), free CBD, and CBD-NL. Representative histopathological alterations are indicated by arrows, including tissue degeneration, increased inflammatory cell density, and vacuolization. The CBD-NL-treated group showed relatively improved tissue architecture with fewer pathological changes compared with the CBD and Blank-NL groups. Representative images are shown; n = 7 rats per group. Images were acquired at ×400 magnification (scale bar = 10 μm). Representative images are shown; n = 7 rats per group.

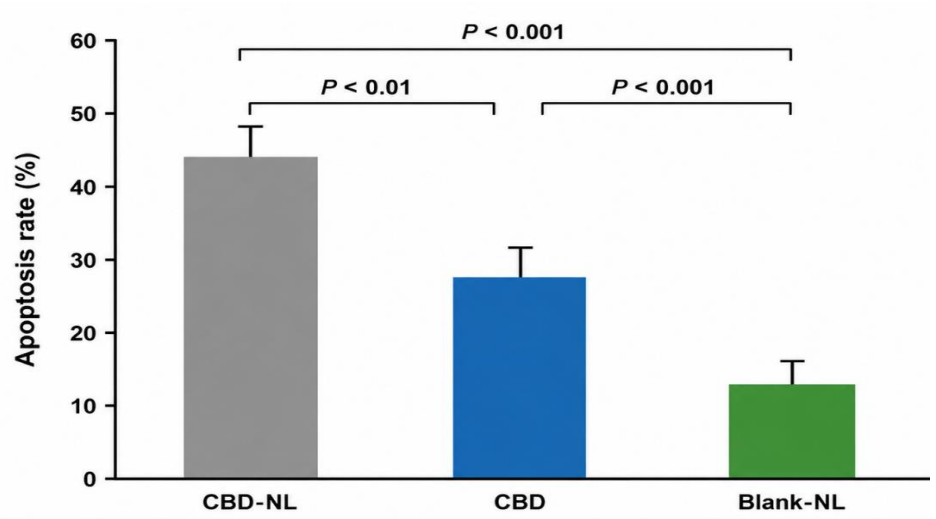

Figure 4. Apoptosis rate in rat brain tissue from the glioblastoma model induced with C6 glioma cells and treated with blank nanoliposome (Blank-NL), free cannabidiol (CBD), or CBD-loaded nanoliposome (CBD-NL). Statistical significance among groups is shown by connecting lines above the bars with the corresponding P values. Pairwise comparisons were performed using one-way ANOVA followed by Tukey's HSD post-hoc test. Data are presented as mean ± SD; n = 7 rats per group.

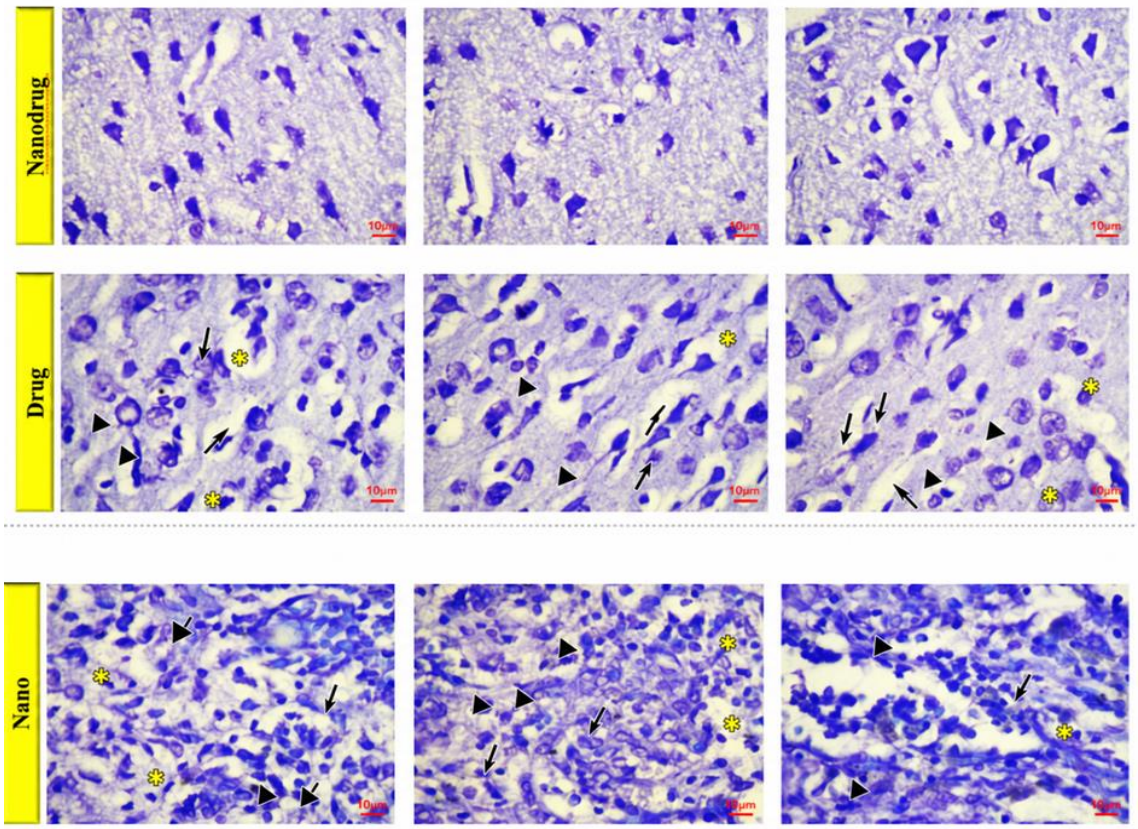

Figure 5. Cresyl Violet-stained sections of rat brain tissue from glioblastoma-bearing rats treated with CBD-loaded nanoliposome (CBD-NL), free cannabidiol (CBD), and blank nanoliposome (Blank-NL). Arrows indicate tissue degeneration, arrowheads indicate higher density of inflammatory cells, and asterisks indicate vacuolization. The CBD-NL-treated group showed relatively preserved tissue architecture compared with the CBD and Blank-NL groups. Representative images were acquired at ×400 magnification (scale bar = 10 μm). Representative images are shown; n = 7 rats per group.

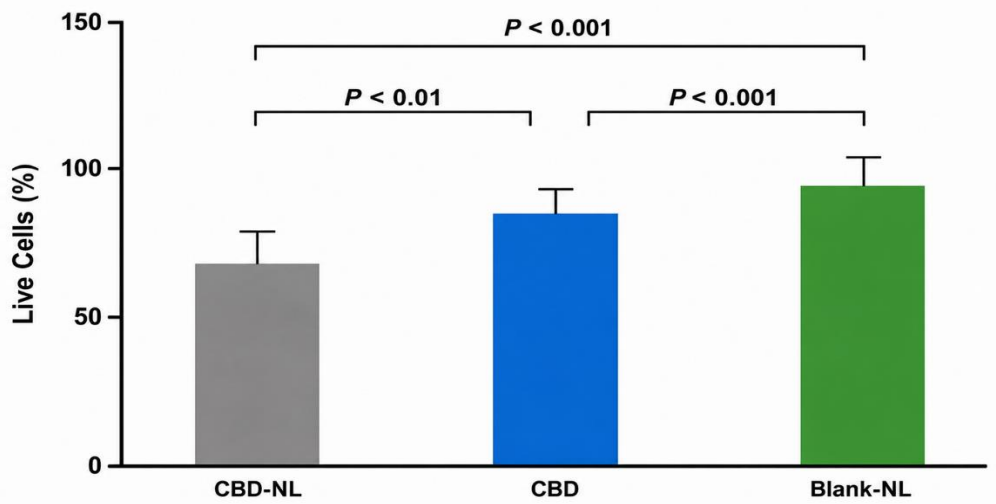

Figure 6. Percentage of live cells in rat brain tissue from the glioblastoma model induced with C6 glioma cells and treated with CBD-loaded nanoliposome (CBD-NL), free cannabidiol (CBD), or blank nanoliposome (Blank-NL). Statistical significance among groups is shown by connecting lines above the bars with the corresponding P values. Pairwise comparisons were performed using one-way ANOVA followed by Tukey's HSD post-hoc test. Data are presented as mean ± SD; n = 7 rats per group.

The relative mRNA expression of RIPK3, VDCA1, TNF-α, and IL-6 in rat brain tissue from the glioblastoma model (induced with C6 glioma cells), in rats treated with cannabidiol, and in rats treated with cannabidiol-loaded nanoliposomes, relative to the control gene GADPH, is shown in Figures 7, 8, 9, and 10, respectively. As is evident, the mRNA expression levels of RIPK3, VCDA1, TNF-α, and IL-6 in the tumor-model rats treated with both cannabidiol and the cannabidiol-loaded liposome decreased significantly compared with the model rats ($p<0.001$). Moreover, the changes in the expression of the above-mentioned genes in rats treated with the cannabidiol-loaded liposome were significant compared with the cannabidiol-treated group ($p<0.001$).

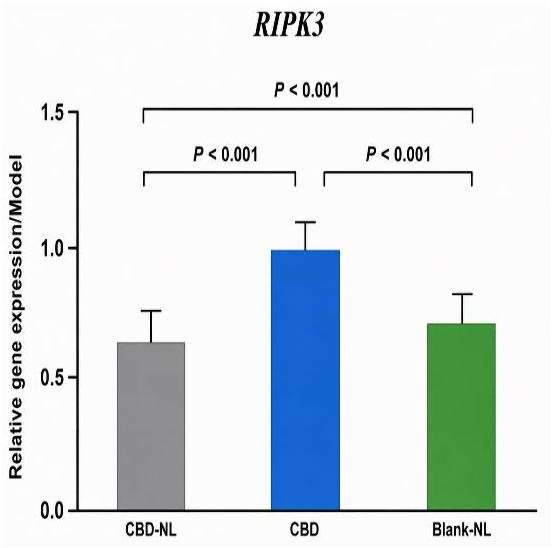

Figure 7. Relative mRNA expression of *RIPK3* in rat brain tissue from the glioblastoma model induced with C6 glioma cells and treated with free CBD-loaded nanoliposome (CBD-NL), free cannabidiol (CBD), or blank nanoliposome (Blank-NL), normalized to GAPDH. Statistical significance among groups is shown by connecting lines above the bars with the corresponding p values, based on one-way ANOVA followed by Tukey's HSD post-hoc test. Data are presented as mean ± SD; n = 7 rats per group.

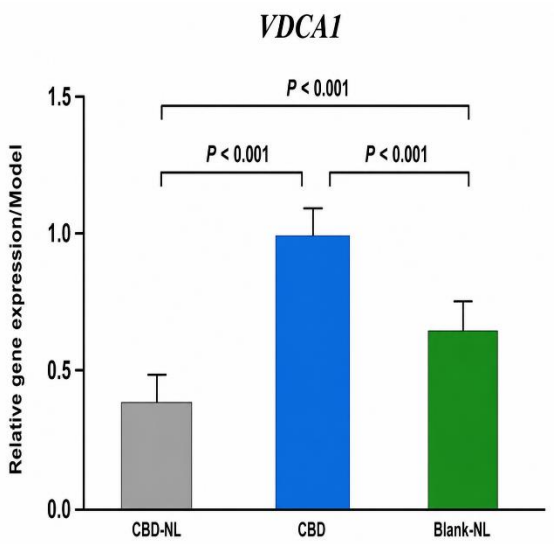

Figure 8. Relative mRNA expression of *VDAC1* in rat brain tissue from the glioblastoma model induced with C6 glioma cells and treated with free CBD-loaded nanoliposome (CBD-NL), free cannabidiol (CBD), or blank nanoliposome (Blank-NL), normalized to GAPDH. Statistical significance among groups is shown by connecting lines above the bars with the corresponding p values, based on one-way ANOVA followed by Tukey's HSD post-hoc test. Data are presented as mean ± SD; n = 7 rats per group.

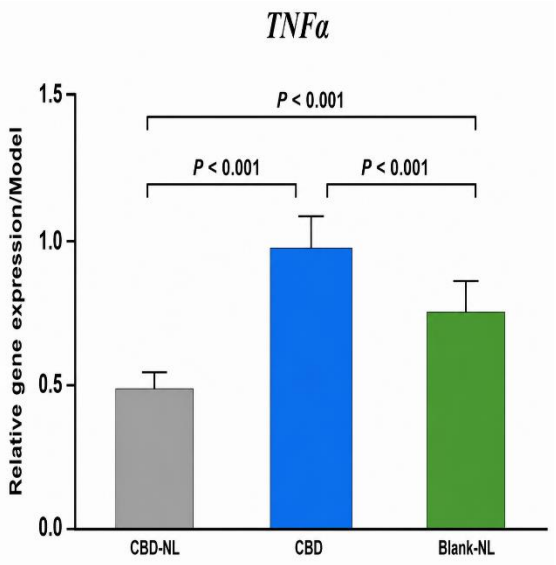

Figure 9. Relative mRNA expression of *TNFα* in rat brain tissue from the glioblastoma model induced with C6 glioma cells and treated with free CBD-loaded nanoliposome (CBD-NL), free cannabidiol (CBD), or blank nanoliposome (Blank-NL), normalized to GAPDH. Statistical significance among groups is shown by connecting lines above the bars with the corresponding p values, based on one-way ANOVA followed by Tukey's HSD post-hoc test. Data are presented as mean ± SD; n = 7 rats per group

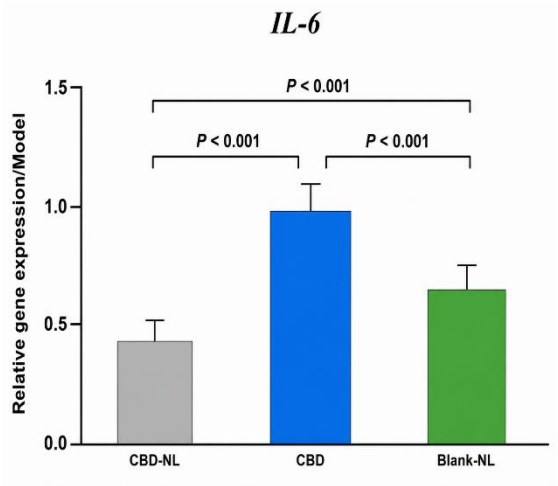

Figure 10. Relative mRNA expression of *IL-6* in rat brain tissue from the glioblastoma model induced with C6 glioma cells and treated with CBD-loaded nanoliposome (CBD-NL), free cannabidiol (CBD), or blank nanoliposome (Blank-NL), normalized to GAPDH. Statistical significance among groups is shown by connecting lines above the bars with the corresponding p values, based on one-way ANOVA followed by Tukey's HSD post-hoc test. Data are presented as mean ± SD; n = 7 rats per group.

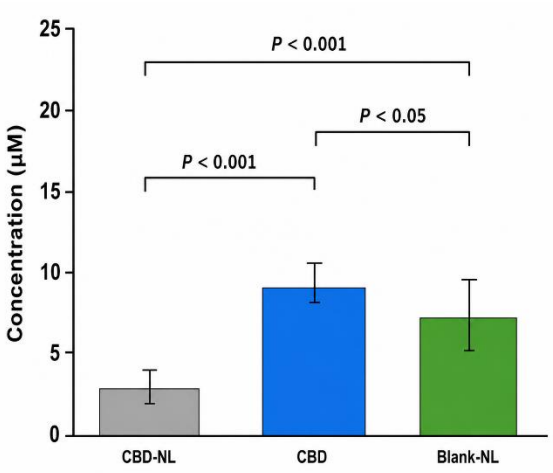

Figure 11. MDA level in rat brain tissue from the glioblastoma model (induced with C6 glioma cells), and treated with CBD-loaded nanoliposome (CBD-NL), free cannabidiol (CBD), or blank nanoliposome (Blank-NL). Statistical significance among groups is shown by connecting lines above the bars with the corresponding p values, based on one-way ANOVA followed by Tukey's HSD post-hoc test. Data are presented as mean ± SD; n = 7 rats per group.

Results of antioxidant enzyme assays

The activities of the antioxidant enzyme MDA and the lipid-peroxidation marker SOD in rat brain tissue from the glioblastoma model (induced with C6 glioma cells), the CBD-treated group, and the CBD-NL–treated group are shown in Figure 11 and 12, respectively. According to these graphs, SOD activity increased and MDA levels decreased in both treatment groups compared with the tumor model rats ($p<0.001$). Moreover, the reported changes in SOD and MDA in the CBD- -NL group were significant compared with the CBD-only group ($p<0.05$).

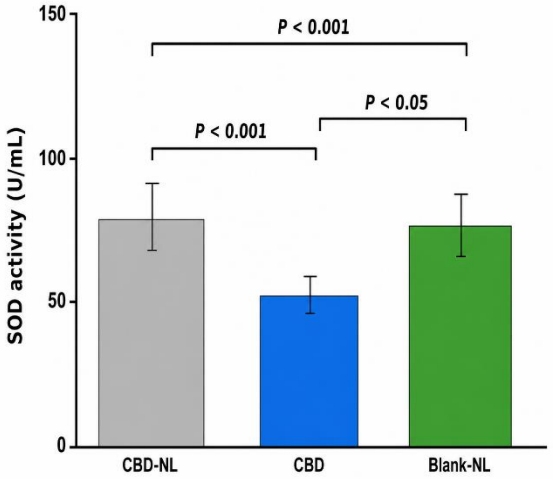

Figure 12. SOD (superoxide dismutase) activity in rat brain tissue from the glioblastoma model (induced with C6 glioma cells), and treated with CBD-loaded nanoliposome (CBD-NL), free cannabidiol (CBD), or blank nanoliposome (Blank-NL). Statistical significance among groups is shown by connecting lines above the bars with the corresponding p values, based on one-way ANOVA followed by Tukey's HSD post-hoc test. Data are presented as mean ± SD; n = 7 rats per group.

Discussion

This study demonstrates that engineering a cannabidiol-loaded nanoliposome (CBD-NL) yields a nanoscale, morphologically uniform carrier (~50 nm by DLS; spherical by SEM/TEM) with FTIR features consistent with non-covalent drug–lipid interactions. FTIR retention of phospholipid head-group bands alongside CBD O–H/C–O/aromatic signatures argues for encapsulation/partitioning rather than chemical derivatization, a prerequisite for translation in CNS delivery. The band near 719 cm^{-1} was interpreted cautiously because it may overlap with lipid CH_2 rocking vibrations and is not specific only to CBD. The shifts and intensity changes observed in the 3600–1600 cm^{-1} region, particularly in O–H, C–H, C=O, and aromatic/C=C bands, suggest non-covalent interactions between CBD and the liposomal components, supporting successful encapsulation without chemical degradation of CBD (Šturm and Poklar Ulrih 2021; Limongi et al. 2021). This interpretation is important because preservation of the main CBD spectral features suggests that the formulation process did not chemically alter the active compound, while the observed band shifts support physical incorporation of CBD within the lipid bilayer. Such behavior is commonly expected in lipid vesicular systems where hydrophobic molecules partition into lipid domains and interact with phospholipid chains or polar head groups without forming new covalent bonds.

Such physicochemical features are in line with current lipid-based nanocarriers developed for glioblastoma which are designed to stabilize hydrophobic actives, prolong circulation, and improve BBB crossing (Kulkarni et al. 2025). Liposomal and other lipid nanoparticle systems have repeatedly been shown to increase intratumoral drug accumulation and sharpen therapeutic indices relative to free drugs in preclinical neuro-oncology models (Si et al. 2025). The small particle size observed in the present formulation may be particularly relevant for brain-tumor delivery, as nanoscale lipid carriers can improve drug dispersion, protect lipophilic compounds from early degradation, and increase the probability of interaction with tumor-associated vascular and cellular barriers. Recent reports on CBD-loaded lipid and liposomal formulations have similarly emphasized that nanoscale encapsulation can improve CBD stability, cellular uptake, and anti-glioblastoma activity compared with non-encapsulated CBD (Xie et al. 2024; Rybarczyk et al. 2025).

In vivo, CBD-NLs clearly outperformed free CBD across histopathological endpoints. Rats treated with CBD-NLs exhibited more pronounced tumor regression on H&E staining and better preservation of neuronal architecture on Cresyl Violet compared with both untreated glioma controls and the free-CBD group. These findings are consistent with accumulating evidence that CBD can restrain proliferation, mitochondrial function and promotes apoptosis in glioma cells, effects that are amplified when CBD is delivered in optimized nanoformulations or combined with conventional therapies such as temozolomide (Feng et al. 2024). The histological improvement observed in the CBD-NL group may reflect the combined benefit of CBD biological activity and improved nanoliposomal delivery. In glioblastoma, tissue destruction, cellular atypia, inflammatory infiltration, and vacuolization are linked to the aggressive invasive behavior of the tumor and its inflammatory microenvironment. Therefore, the reduction of these pathological changes in treated animals supports a tissue-level therapeutic effect rather than an isolated molecular change.

The pro-apoptotic profile observed in the CBD-NL group is mechanistically plausible. CBD has been shown to perturb mitochondrial function, calcium homeostasis, and DNA-repair machinery

(e.g. RAD51), thereby facilitating apoptotic cell death and chemosensitization in glioblastoma models (Soroceanu et al. 2022). The downregulation of Voltage-Dependent Anion Channel 1 (*VDAC1*) seen here aligns with the pivotal role of this outer mitochondrial membrane channel as a "gatekeeper" of mitochondrial metabolism, ion flux, and apoptosis. Overexpression of VDAC1 is documented in glioblastoma and is associated with enhanced metabolic plasticity and resistance to cell death; its targeting can shift tumor cells toward apoptosis and decrease tumor growth (Shoshan-Barmatz et al. 2020). Thus, the reduction in VDAC1 transcript levels in CBD-NL–treated animals may reflect a broader normalization of mitochondrial control points, in line with recent data implicating VDAC1 in CBD-mediated cancer cell death (Melo et al. 2025).

The redox and inflammatory profiles observed further support a multi-axis mechanism. Restoration of SOD activity together with reduced MDA indicates attenuation of oxidative stress and lipid peroxidation—processes strongly implicated in glioblastoma progression and in sustaining pro-survival signaling pathways (Ullah et al. 2021). This finding is also supported by recent evidence indicating that oxidative stress contributes to glioblastoma proliferation, survival, immune evasion, metabolic adaptation, and treatment resistance. Therefore, the increase in SOD and reduction in MDA observed in the CBD-NL group suggest that this formulation may reduce tumor-associated oxidative injury and help restore redox balance within the brain tumor microenvironment (Nowacka et al. 2025). Concurrent down-regulation of TNF-α and IL-6 suggests that CBD-NLs dampen key cytokine networks that drive glioma proliferation, invasion, and immune evasion (Liu et al. 2024). Both TNF-α and IL-6 are known to promote reactive oxygen species generation, PI3K/AKT signaling, and a protumorigenic microenvironment in glioblastoma (Lin et al. 2024; Volmar 2019). Recent work also supports the role of inflammatory cytokine signaling, including IL-6-related pathways and *TNF-α* associated inflammatory responses, in sustaining glioma growth and a stress-tolerant tumor microenvironment (Bao et al. 2025).

Importantly, the magnitude of change in these markers—histological regression, increased apoptosis, SOD and MDA normalization, and suppression of *TNF-α*, *IL-6*, *RIPK3*, and *VDAC1*—was consistently greater with CBD-NL than with free CBD. This pattern strongly supports the central premise of the work: enhancing delivery and brain exposure of CBD through a rationally designed nanoliposomal carrier unlocks more of its intrinsic antitumor potential. These findings resonate with recent nanomedicine studies where CBD-containing liposomal formulations or other lipid nanocarriers achieved stronger anti-glioblastoma effects and improved selectivity compared with non-encapsulated CBD in cell and animal models (Rybarczyk et al. 2025). Thus, the present results suggest that the superior effect of CBD-NLs is not limited to one endpoint but is reflected across structural, apoptotic, oxidative, inflammatory, and gene-expression outcomes. This coordinated response supports the view that CBD-NLs act through a multi-target mechanism involving improved delivery, enhanced tumor-cell stress, suppression of inflammatory signaling, and partial restoration of antioxidant defense.

A limitation of this study is that pre-treatment tumor-size assessment by imaging was not performed, brain sections from all groups at the time of treatment initiation were not available, and tumor size or tumor weight were not directly quantified. Therefore, treatment efficacy was evaluated based on endpoint histopathological changes, apoptosis rate, oxidative-stress markers, and inflammatory and necroptotic gene-expression outcomes. Representative apoptotic-cell images and quantitative apoptotic-cell data for the

untreated glioblastoma group were not available from the original experiment; therefore, these data could not be added retrospectively. A further limitation of this study is that survival analysis was not performed, as animals were euthanized at predefined experimental endpoints for histological, biochemical, and molecular assessments. Therefore, survival outcomes could not be evaluated in the present experimental design.

Also this study recommended a future work in Priorities include (i) quantitative pharmacokinetics (PK) (intratumoral CBD, brain/plasma ratios) and biodistribution, (ii) dose-finding and toxicity mapping, (iii) combination therapy (with TMZ/radiation; schedule optimization), (iv) expansion to patient-derived xenografts, and (v) proteomic/metabolomic profiling to map pathway rewiring under CBD-NL pressure.

Pairing a polyvalent pharmacological compound, CBD, with a blood–brain barrier aware nanoliposomal carrier produced significant therapeutic and molecular benefits in an orthotopic GBM rat model. The CBD-NL formulation demonstrated superior performance compared with free CBD, leading to pronounced histopathological regression, enhanced apoptotic signaling, and normalization of redox balance—as evidenced by increased SOD activity and reduced MDA levels.

Furthermore, treatment with CBD-NL effectively suppressed inflammatory TNF-α, IL-6 and necroptotic RIPK3, VDAC1 gene axes. These findings indicate that combining a pleiotropic bioactive molecule with a rationally engineered nanocarrier can overcome the dual limitations of pharmacologic exposure and therapeutic resistance that typify GBM.

Collectively, the results reinforce the central paradigm that delivery-mechanism innovation—achieved through nanoscale, BBB-permeable carriers should be considered a foundational complement to molecular targeting strategies in GBM therapy.

Acknowledgment

The authors would like to thank the Department of Biology, Central Tehran Branch, Islamic Azad University, Tehran, Iran, for providing laboratory facilities and technical support. The authors also acknowledge the Iran National Cell Bank for supplying the C6 glioma cell line used in this study.

Conflicts of interest

The authors had no competing interests.

Funding

This research received no external funding.

Ethical Considerations

All experimental procedures involving animals were conducted in accordance with the European Directive 2010/63/EU, the AVMA Guidelines for the Euthanasia of Animals (2020), and the ARRIVE guidelines. Every effort was made to minimize animal suffering and to reduce the number of animals used in the study.

Code of Ethics

The study protocol was approved by the Animal Care and Use Committee of Islamic Azad University, Central Tehran Branch, Faculty of Basic Sciences (Approval No. 75384/87; Date: 22 March 2021).

Authors' Contributions

Zahraa Abdulalamir conceived and designed the study, performed the experiments, analyzed the data, and drafted the manuscript. Zahra Keshtmand supervised the study, contributed to the experimental design, interpreted the results, critically revised the manuscript, and approved the final version for publication.

Abbreviations

- BBB: Blood–Brain Barrier
- CBD: Cannabidiol

- CBD-NL: Cannabidiol-Loaded Nanoliposome
- CNS: Central Nervous System
- DLS: Dynamic Light Scattering
- DMEM: Dulbecco's Modified Eagle Medium
- DSPC: 1,2-Distearoyl-sn-glycero-3-phosphocholine
- FTIR: Fourier Transform Infrared Spectroscopy
- GBM: Glioblastoma Multiforme
- H&E: Hematoxylin and Eosin
- IL-6: Interleukin-6
- MDA: Malondialdehyde
- NCS: Newborn Calf Serum
- PDI: Polydispersity Index
- RIPK3: Receptor-Interacting Serine/Threonine-Protein Kinase 3
- RT-qPCR: Reverse Transcription Quantitative Polymerase Chain Reaction
- SEM: Scanning Electron Microscopy
- SOD: Superoxide Dismutase
- TEM: Transmission Electron Microscopy
- TMZ: Temozolomide
- TNF-α: Tumor Necrosis Factor-Alpha
- VDAC1: Voltage-Dependent Anion Channel 1

References

Angom RS, Nakka NMR, Bhattacharya S (2023) Advances in glioblastoma therapy: an update on current approaches. Brain Sci 13(11):1536

Banerjee S, Saharan VA, Banerjee D, et al (2024) A comprehensive update on cannabidiol, its formulations and drug delivery systems. Phytochem Rev:1–35

Bao Y, et al (2025) From neuroinflammation to gliomagenesis: immune drivers of glioma initiation and progression. Mol Cancer 24:Article number not specified

Barth RF, Kaur B (2009) Rat brain tumor models in experimental neuro-oncology: the C6, 9L, T9, RG2, F98, BT4C, RT-2 and CNS-1 gliomas. J Neurooncol 94(3):299–312

Bukowska B (2024) Current and potential use of biologically active compounds derived from Cannabis sativa L. in the treatment of selected diseases. Int J Mol Sci 25(23):12738

Chauhan AS, Chand P, Parashar T (2025) Lipid-based nanoparticles: strategy for targeted cancer therapy. BIO Integr 6(1):994

Danaei M, Dehghankhold M, Ataei S, Hasanzadeh Davarani F, Javanmard R, Dokhani A, Khorasani S, Mozafari MR (2018) Impact of particle size and polydispersity index on the clinical applications of lipidic nanocarrier systems. Pharmaceutics 10(2):57

Directive E (2010) Directive 2010/63/EU of the European Parliament and of the Council of 22 September 2010 on the protection of animals used for scientific purposes. Off J Eur Union 276:33–79

Doonan F, Cotter TG (2008) Morphological assessment of apoptosis. Methods 44(3):200–204

Elmore S (2007) Apoptosis: a review of programmed cell death. Toxicol Pathol 35(4):495–516

Fekete B (2024) Survival of patients with glioblastoma-advancements in the past two decades

Feng S, Pan Y, Lu P, Li N, Zhu W, Hao Z (2024) From bench to bedside: the application of cannabidiol in glioma. J Transl Med 22(1):648

Filippov SK, Khusnutdinov R, Murmiliuk A, Inam W, Zakharova LY, Zhang H, Khutoryanskiy VV (2023) Dynamic light scattering and transmission electron microscopy in drug delivery: a roadmap for correct characterization of nanoparticles and interpretation of results. Mater Horiz 10(12):5354–5371

Fischer AH, Jacobson KA, Rose J, Zeller R (2008) Hematoxylin and eosin staining of tissue and cell sections. Cold Spring Harb Protoc 2008(5):pdb.prot4986

Giakoumettis D, Kritis A, Foroglou N (2018) C6 cell line: the gold standard in glioma research. Hippokratia 22(3):105–112

Gilard V, Tebani A, Dabaj I, et al (2021) Diagnosis and management of glioblastoma: a comprehensive perspective. J Pers Med 11(4):258

Grifoni L, Landucci E, Pieraccini G, et al (2025) Development and blood–brain barrier penetration of nanovesicles loaded with cannabidiol. Pharmaceuticals (Basel) 18(2):160

Gross C, Ramirez DA, McGrath S, Gustafson DL (2021) Cannabidiol induces apoptosis and perturbs mitochondrial function in human and canine glioma cells. Front Pharmacol 12:725136

Guo T, Wu C, Zhang J, et al (2023) Dual blockade of EGFR and PI3K signaling pathways offers a therapeutic strategy for glioblastoma. Cell Commun Signal 21(1):363

Hammond L (2023) Cresyl violet staining (Nissl staining). The Open Lab Book

Hasan N, Imran M, Sheikh A, et al (2022) Cannabis as a potential compound against various malignancies, legal aspects, advancement by exploiting nanotechnology and clinical trials. J Drug Target 30(7):709–725

Hersh AM, Alomari S, Tyler BM (2022) Crossing the blood-brain barrier: advances in nanoparticle technology for drug delivery in neuro-oncology. Int J Mol Sci 23(8):4153

Hossain KR, Alghalayini A, Valenzuela SM (2023) Current challenges and opportunities for improved cannabidiol solubility. Int J Mol Sci 24(19):14514

Khalighi S, Reddy K, Midya A, Pandav KB, Madabhushi A, Abedalthagafi M (2024) Artificial intelligence in neuro-oncology: advances and challenges in brain tumor diagnosis, prognosis, and precision treatment. NPJ Precis Oncol 8(1):80

Khot S, Krishnaveni A, Gharat S, Momin M, Bhavsar C, Omri A (2024) Innovative drug delivery strategies for targeting glioblastoma: overcoming the challenges of the tumor microenvironment. Expert Opin Drug Deliv 21(12):1837–1857

Kulkarni M, Nadendla K, Pai A, Ashili S, Maibach H, Manikkath J (2025) Lipid nanoparticles for treatment of glioblastoma multiforme: current status of research and clinical translation. J Drug Deliv Sci Technol:106891

Li S, Wang L, Han M, et al (2025) Combination of sodium butyrate and immunotherapy in glioma: regulation of immunologically hot and cold tumors via gut microbiota and metabolites. Front Immunol 16:1532528

Limongi T, Susa F, Marini M, et al (2021) Lipid-based nanovesicular drug delivery systems. Nanomaterials (Basel) 11(12):3391

Lin H, Liu C, Hu A, Zhang D, Yang H, Mao Y (2024) Understanding the immunosuppressive microenvironment of glioma: mechanistic insights and clinical perspectives. J Hematol Oncol 17(1):31

Liu Y, Zhou F, Ali H, Lathia JD, Chen P (2024) Immunotherapy for glioblastoma: current state, challenges, and future perspectives. Cell Mol Immunol 21(12):1354–1375

Livak KJ, Schmittgen TD (2001) Analysis of relative gene expression data using real-time quantitative PCR and the 2−ΔΔCT method. Methods 25(4):402–408

Louis DN, Perry A, Wesseling P, et al (2021) The 2021 WHO classification of tumors of the central nervous system: a summary. Neuro Oncol 23(8):1231–1251

Melo ES, Asevedo EA, Duarte-Almeida JM, et al (2025) Mechanisms of cell death induced by cannabidiol against tumor cells: a review of preclinical studies. Plants (Basel) 14(4):585

Nowacka A, Kubiak K, Żuryń A, et al (2025) Oxidative stress and antioxidants in glioblastoma: mechanisms of action, therapeutic effects and future directions. Antioxidants (Basel) 14(9):1121

Oleszko A, Olsztyńska-Janus S, Walski T, Grzeszczuk-Kuć K, Bujok J, Gałecka K, Czerski A, Witkiewicz W, Komorowska M (2015) Application of FTIR-ATR spectroscopy to determine the extent of lipid peroxidation in plasma during haemodialysis. Biomed Res Int 2015:245607

Price M, Ballard C, Benedetti J, et al (2024) CBTRUS statistical report: primary brain and other central nervous system tumors diagnosed in the United States in 2017–2021. Neuro Oncol 26(Suppl 6):vi1

Rehman M, Tahir N, Sohail MF, et al (2024) Lipid-based nanoformulations for drug delivery: an ongoing perspective. Pharmaceutics 16(11):1376

Rybarczyk A, Majchrzak-Celińska A, Piwowarczyk L, Krajka-Kuźniak V (2025) The anti-glioblastoma effects of novel liposomal formulations loaded with cannabidiol, celecoxib, and 2,5-dimethylcelecoxib. Pharmaceutics 17(8):1031

Senjab RM, Almutairi MM, Alrufayi M, et al (2024) Advances in liposomal nanotechnology: from concept to clinics. RSC Pharm 1(4):556–578

Shi J, Zhang Y, Wang J, et al (2015)

Establishment of C6 brain glioma models through stereotactic technique for laser interstitial thermotherapy research. Surg Neurol Int 6:51

Shoshan-Barmatz V, Shteinfer-Kuzmine A, Verma A (2020) VDAC1 at the intersection of cell metabolism, apoptosis, and diseases. Biomolecules 10(11):1485

Si JX, Liu ZC, Gu F, Jin X, Ma YY (2025) Nanoparticle-based delivery systems for targeted therapy in brain tumors: progress, challenges and perspectives. Int J Oncol 67(4):1–15

Soroceanu L, Singer E, Dighe P, et al (2022) Cannabidiol inhibits RAD51 and sensitizes glioblastoma to temozolomide in multiple orthotopic tumor models. Neurooncol Adv 4(1):vdac019

Stupp R, Hegi ME, Mason WP, et al (2009) Effects of radiotherapy with concomitant and adjuvant temozolomide versus radiotherapy alone on survival in glioblastoma in a randomised phase III study: 5-year analysis of the EORTC-NCIC trial. Lancet Oncol 10(5):459–466

Šturm L, Poklar Ulrih N (2021) Basic methods for preparation of liposomes and studying their interactions with different compounds, with the emphasis on polyphenols. Int J Mol Sci 22(12):6547

Trivedi MK, Branton A, Trivedi D, Mondal S, Jana S (2023) Cannabidiol (CBD) upregulates vitamin D3 receptors (VDRs) expression that modulates cytokines (TNF-α, IL-6), tissue elasticity, cellular senescence, and mitochondrial ATP generation in human and rodent cell lines. Nutr Diet Suppl:91–100

Ullah H, Di Minno A, Santarcangelo C, Khan H, Daglia M (2021) Improvement of oxidative stress and mitochondrial dysfunction by β-caryophyllene: a focus on the nervous system. Antioxidants (Basel) 10(4):546

Volmar MNM (2019) Cannabidiol for glioblastoma therapy: models, molecular pathways, and predictive markers. Dissertation, Ludwig-Maximilians-Universität München, Munich

Wu D, Chen Q, Chen X, Han F, Chen Z, Wang Y (2023) The blood–brain barrier: structure, regulation and drug delivery. Signal Transduct Target Ther 8(1):217

Xie Y, Li P, Fu D, et al (2024) CBD-loaded nanostructured lipid carriers: optimization, characterization, and stability. ACS Omega 9(39):40632–40643

Yabo YA, Niclou SP, Golebiewska A (2022) Cancer cell heterogeneity and plasticity: a paradigm shift in glioblastoma. Neuro Oncol 24(5):669–682

Yau GTY, Tai W, Arnold JC, Chan HK, Kwok PCL (2023) Cannabidiol for the treatment of brain disorders: therapeutic potential and routes of administration. Pharm Res 40(5):1087–1114

Zaidi SE, Moelker E, Singh K, et al (2023) Novel immunotherapeutic approaches for the treatment of glioblastoma. BioDrugs 37(4):489

Zapata K, Rosales S, Rios A, et al (2023) Nanoliposomes for controlled release of cannabinodiol at relevant gastrointestinal conditions. ACS Omega 8(46):43698–43707